We are IntechOpen, the world's leading publisher of Open Access books Built by scientists, for scientists

4,800
Open access books available

122,000
International authors and editors

135M
Downloads

Our authors are among the

154
Countries delivered to

TOP 1%
most cited scientists

12.2%
Contributors from top 500 universities

CLARIVATE ANALYTICS BOOK CITATION INDEX INDEXED

WEB OF SCIENCE™

Selection of our books indexed in the Book Citation Index in Web of Science™ Core Collection (BKCI)

Interested in publishing with us?
Contact book.department@intechopen.com

Numbers displayed above are based on latest data collected.
For more information visit www.intechopen.com

7

Lattice Boltzmann Modeling for Melting/Solidification Processes

Dipankar Chatterjee
CSIR-Central Mechanical Engineering Research Institute
India

1. Introduction

The phenomena of melting and solidification are associated with many practical applications, such as metal processing, castings, environmental engineering, thermal energy storage system in space station and many more. In these processes, matter is subject to a change of phase and consequently, a boundary separating two different phases evolves and moves within the matter. Mathematical modeling of such 'moving boundary problems' are always a challenging task because of the dynamic evolution of the phase separating boundary, complex boundary conditions as well as varying thermophysical properties. Many macroscopic mathematical modeling strategies for the solidification/melting problems can be found in the contemporary literatures. An excellent review in this regard can be found in Hu & Argyropoulos (1996). Early efforts in melting/solidification modeling initiated with a moving/deforming grid approach (Rubinsky & Cravahlo, 1981; Voller & Cross, 1981; Voller & Cross, 1983; Weaver & Viskanta, 1986; Askar, 1987), in which independent conservation equations for each phase need to be initially formulated, and are to be subsequently coupled with appropriate boundary conditions at the inter-phase interfaces. However, such multiple region solutions require the existence of discrete interfaces between the respective phases. In fact, a major difficulty with regard to their implementation is associated with tracking of the phase interfaces (which are generally unknown functions of space and time). The need for moving numerical grids and/or coordinate mapping procedures complicates the application of this technique further, and generally, simplifying assumptions regarding the geometric regularity of the interfaces are made. Additionally, a serious limitation exists for modeling phase change behavior of multi-component systems, since, unlike pure substances; such systems do not exhibit a sharp interface between solid and liquid phases, in a macroscopic sense. The phase-change behavior of such systems depends on many factors including the phase-change environment, composition, and thermodynamic descriptions of specific phase transformations. Moreover, solidification occurs over extended temperature ranges and solid formation often occurs as a permeable crystalline-like matrix which coexists with the liquid phase. In such cases, it would be virtually impossible to track a morphologically complex zone in a macroscopic framework, using any moving grid technique. In contrast, in fixed-grid mathematical models of phase change (Comini et al., 1974; Morgan et al., 1978; Roose & Storrer, 1984; Dalhuijsen & Segal, 1986; Pham, 1986; Dhatt et al., 1989; Comini et al., 1990; Voller et al., 1990), transport equations for individual phases are volume-averaged to

come up with equivalent single-phase conservation equations that are valid over the entire domain, irrespective of the constituent phases locally present. A separate equation for evolution of liquid fraction is solved in conjunction with the above set of conservation equations, which implicitly specifies and updates the interfacial locations with respect to space and time.

It can be noted at this point that although simulation strategies mentioned as above have become somewhat standardized over the past few decades, solution of phase-change problems over multiple length scales still poses serious challenges, primarily because of the disparate and coupled length scales characterizing the entire sequence of transport processes. To overcome such difficulties, phase-field models of dendritic solidification have been developed and proposed by several researchers (Mikheev & Chernov, 1991; Kim et al., 1999; Harrowell & Oxtoby, 1987; Khachaturyan, 1996; Beckermann et al., 1999; Tong et al., 2001). Advantage of the phase field models lies in the fact that computational difficulties associated with front tracking are eliminated by introducing an auxiliary order parameter (the so-called phase field) that couples with the evolution of the thermal field. Dynamics of the phase field are designed to follow the evolving solidification front, thereby eliminating the necessity of any explicit front tracking.

Recently, the multiscale mesoscopic lattice Boltzmann (LB) (Kendon et al., 2001; Sankaranarayanan et al., 2002; Barrios et al., 2005) method has emerged to offer huge potentials for solving complex thermofluidic problems involving morphological development of complicated phase boundaries such as the problem of phase separation of two immiscible fluids (Chen & Doolen, 1998). Such a method, typically, considers volume elements of fluid comprising of a collection of particles that are represented by characteristic particle velocity distribution functions defined at discrete grid points. The rules governing the collisions and subsequent relaxations are designed such that the time-averaged motion of fluid particles becomes consistent with that predicted by the Navier-Stokes equation. Further advancements in LB modeling of fluid flow enabled the research community to explore more complicated problems addressing flow through porous medium and a few generic cases of multi-phase flow (Gunstensen et al., 1991; Shan & Chen, 1993; Ferreol & Rothman, 1995). In this context, it can be mentioned here that a distinct advantage of the LB method for modeling solid-liquid phase transitions, in comparison to a classical continuum based formulation, lies in the fact that the LB method is fundamentally based on microscopic particle models and mesoscopic kinetic equations, which means that micro and meso-scale physics of phase transitions can elegantly be incorporated. Another important advantage is that it does not require an immediate explicit calculation of fluid pressure, leading to time-efficient computational simulations. Further, LB models are inherently parallelizable, which renders their suitability to address phase change processes over large-scale computational domains.

The LB approaches proposed so far for modeling solid-liquid phase transition problems can broadly be categorized into two major groups, *viz*. (a) phase field based methods following the Ginzburg-Landau theory and (b) enthalpy based methods. De Fabritiis et al. (1998) developed a thermal LB model for such problems by employing two types of quasiparticles for solid and liquid phases, respectively. Miller et al. (2001) proposed a simple reaction LB model with enhanced collisions, using a single type of quasiparticle and a phase field approach. Further work proceeded along similar lines (Miller & Schroder, 2001; Miller, 2001; Miller & Succi, 2002; Miller et al., 2004; Rasin et al., 2005; Medvedev & Kassner, 2005), with

the phase-field model acting as a pivotal basis for determining the evolution of respective phase fractions. It needs to be emphasized that one of the major problems in implementing the phase field based methods in the context of solid-liquid phase transition problems is the requirement of limitlingly finer grid spacing for resolving the interfacial region to reproduce the dynamics of the sharp interface equations. Consequently, adaptive mesh refinement strategies involving computationally involved data structures are required for problems subjected to small undercooling. On the other hand, enthalpy-based models have been extensively used to solve complex solidification problems over macroscopic and mesoscopic length scales. An extended LB methodology, in conjunction with an enthalpy formulation for treatment of solid–liquid phase change aspects in case of diffusion dominated problems, was first introduced by Jiaung et al. (2001). Subsequently, taking the computational advantage of the enthalpy-based technique, Chatterjee & Chakraborty (2005, 2006, 2008), Chakraborty & Chatterjee (2007) and Chatterjee (2009, 2010) proposed a series of LB models primarily applicable to a wide range of melting-solidification problems. It was started with an enthalpy based LB model for diffusion dominated phase transition problems, followed by a hybrid LB method for generalized convection-diffusion transport processes pertinent to melting/solidification problems. In the diffusion models, the temperature field was obtained from an evolution equation of a single particle density distribution function (DF), whereas in the convection-diffusion models the thermal field is described by a novel enthalpy density DF through a kinetic equation based on the total enthalpy of the phase changing system or alternatively from an evolution equation of temperature. The analysis of solidification in a semitransparent material using the enthalpy based LB method was performed by Raj et al. (2006). The radiative component of the energy equation in the LB formulation was computed using the discrete transfer method in their model. Recently, Huber et al. (2008) developed a multiple DF LB model for coupled thermal convection and pure-substance melting, where the two DFs were interrelated through the buoyancy term and the equilibrium DF of the temperature kinetic equation.

In this chapter, we describe a straightforward technique for simulating solid-liquid phase transition, by coupling a passive scalar based thermal LB model with a fixed-grid enthalpy-porosity approach (Brent et al., 1988) that is consistent with the microscopic solvability theory. The macroscopic density and velocity fields are simulated using a single particle density DF through a kinetic equation, while the macroscopic temperature field is obtained from a separate temperature DF through another kinetic equation (Chatterjee, 2010). The phase change aspect is numerically handled by the enthalpy-porosity technique with an adapted enthalpy-updating scheme. The source terms originating out of the physical situation are incorporated into the respective kinetic equations by the most formal technique following the extended Boltzmann equation. Test cases for one and two-dimensional solidification problems are presented and compared with the analytical and available numerical solutions. Finally, simulation results for a popular solid-liquid phase change problem, such as the Bridgman crystal growth in a square crucible are also shown to establish the capability of the model.

2. Model formulation

In this section we first present the generalized convection-diffusion macroscopic conservation equations governing the transport processes occurring during phase change, followed by the corresponding lattice Boltzmann formulation.

2.1 Macroscopic conservation equations

The equivalent single phase volume-averaged macro-scale continuity, momentum and energy conservation equations for a nonparticipating phase changing system, assuming a laminar, incompressible and Newtonian flow, can be presented as:

$$\nabla \cdot \mathbf{u} = 0 \tag{1}$$

$$\rho\left[\partial_t \mathbf{u} + \mathbf{u}.\nabla\mathbf{u}\right] = -\nabla p + \nabla \cdot \boldsymbol{\sigma} + \rho\mathbf{F} \tag{2}$$

$$\rho c_p\left[\partial_t T + \mathbf{u}.\nabla T\right] = \nabla \cdot \left(\kappa \nabla T\right) + \boldsymbol{\sigma} : \nabla\mathbf{u} + \dot{q} \tag{3}$$

where $\mathbf{u}$, p and T denote the macroscopic velocity, pressure and temperature, $\boldsymbol{\sigma} = \rho\nu\left[\left(\nabla\mathbf{u} + \nabla\mathbf{u}^T\right) - 2/3\left(\nabla.\mathbf{u}\right)\mathbf{I}\right]$ is the viscous stress tensor, ρ, ν, c_p and κ are the density, kinematic viscosity, specific heat and thermal conductivity, $\mathbf{F} = \mathbf{G} + \mathbf{S}$ is the body force per unit mass which incorporates a combined contribution form the buoyancy force $\mathbf{G} = \mathbf{g}_a \beta\left(T - T_{ref}\right)$, assuming the Boussinesq approximation to be valid, where $\mathbf{g}_a$ is the acceleration due to gravity, β is the volumetric thermal expansion coefficient and T_{ref} is the reference temperature and a porous medium frictional resistance force $\mathbf{S} = -\left(\nu/\mathbf{K}\right)\cdot\mathbf{u}$, where $\mathbf{K}$ represents the permeability tensor. Components of the tensor $\mathbf{K}$ depend on the specific morphology of the phase changing domain, for which any appropriate formulation for flow through a porous medium can be effectively invoked. A common approach followed in the literature is to adopt the celebrated Darcy model (or some of its variants) for flow through a porous medium, in association with the Cozeny-Karman equation (Voller & Prakash, 1987) as $\mu/\mathbf{K} = M\left(1 - f_l\right)^2 \Big/ \left(f_l^3 + \varepsilon\right)$, where μ is the dynamic viscosity, $M\left(\sim O\left(10^8\right)\right)$ is a morphological constant and $\varepsilon\left(\sim O\left(10^{-3}\right)\right)$ is a computational constant introduced to avoid division by zero. Further, f_l is the liquid fraction, given as $f_l = \Delta h / L$, where L is the latent heat of phase change and Δh is the latent enthalpy content of a computational cell undergoing phase change and can be given by,

$$\begin{aligned} \Delta h &= f(T) = L \quad &: T > T_l \\ &= f_l L \quad &: T_s \le T \le T_l \\ &= 0 \quad &: T < T_s \end{aligned} \tag{4}$$

where T_s and T_l are the solidus and liquidus temperatures respectively.

The above formulation effectively ensures that in the phase changing cells, the porous medium resistance term dominates over the transient, convective and diffusive effects manifested by molecular interaction mechanisms, thereby forcing the velocity field to imitate the Cozeny-Karman law. On the other hand, in totally solid elements $\left(f_l = 0\right)$, the high porous medium resistance forces any velocity predictions effectively to zero. In a fully liquid element $\left(f_l = 1\right)$, however, this term has no consequence, and the usual form of the Navier Stokes equation can be retrieved.

The latent-heat evolution is accounted for by introducing a source term in the macroscopic energy conservation equation (final term on the right-hand side of Eq. (3)) as, $\dot{q} = -\left[\partial_t\left(\rho\Delta h\right) + \nabla.\left(\rho\mathbf{u}\Delta h\right)\right]$. For pure material phase change the term $\nabla.\left(\rho\mathbf{u}\Delta h\right)$ vanishes and the energy source term becomes $\dot{q} = -\partial_t\left(\rho\Delta h\right)$.

2.2 The lattice Boltzmann model

A statistical description of a fluid system can be made in terms of a particle density DF, which satisfies the continuous Boltzmann equation with a single-relaxation-time BGK (Bhatnagar-Gross-Krook) model (Bhatnagar et al., 1954) as:

$$\partial_t f + \boldsymbol{\xi} \cdot \nabla f = -\left(f - f^{eq}\right)\Big/\lambda_f + F \tag{5}$$

where $f(\mathbf{x},\boldsymbol{\xi},t)$ is a single particle density DF from which the macroscopic properties of the fluid can be obtained, $\boldsymbol{\xi}$ is the microscopic velocity, λ_f is the relaxation time, F and $f^{eq}(\mathbf{x},\boldsymbol{\xi},t)$ are the external forcing parameter and the Maxwell-Boltzmann type equilibrium DF, given by,

$$F = \frac{\mathbf{F}.(\boldsymbol{\xi}-\mathbf{u})}{RT} f^{eq}\ ,\ f^{eq} = \frac{\rho}{(2\pi RT)^{D/2}} \exp\left[-\frac{(\boldsymbol{\xi}-\mathbf{u})^2}{2RT}\right] \tag{6}$$

where R is the gas constant and D is the dimensionality. The macroscopic variables are obtained by taking (microscopic velocity) moments of the density DF f as: $\rho = \int f\, d\boldsymbol{\xi}$, $\rho\mathbf{u} = \int f\boldsymbol{\xi}\, d\boldsymbol{\xi} + \rho\mathbf{F}$. However, it is a well known fact that the temperature field obtained from the second moment of the DF f yields a fixed Prandtl number, implying that the thermal diffusivity cannot be adjusted independent of the kinematic viscosity (He et al., 1998), which restricts its applicability to a limited class of problems only.

To this end, we define a new temperature DF $g(\mathbf{x},\boldsymbol{\xi},t)$ following the passive scalar approach of He et al. (1998), which obeys a kinetic equation of the form:

$$\partial_t g + \boldsymbol{\xi} \cdot \nabla g = -\left(g - g^{eq}\right)\Big/\lambda_g + \Re + Q \tag{7}$$

where λ_g is the relaxation time, $g^{eq}(\mathbf{x},\boldsymbol{\xi},t)$ is the is the Maxwell-Boltzmann type equilibrium DF, given by,

$$g^{eq} = \frac{\rho c_p T}{(2\pi RT)^{D/2}} \exp\left[-\frac{(\boldsymbol{\xi}-\mathbf{u})^2}{2RT}\right] = c_p T\, f^{eq} \tag{8}$$

Here $\Re = \Re^I + \Re^{II} + \Re^{III}$ accounts for the viscous heating ($\Re^I$), compression work ($\Re^{II}$) and kinetic energy ($\Re^{III}$) contributions given as (Shi et al., 2004):

$$\Re^I = -\left(f - f^{eq}\right)\left[(\boldsymbol{\xi}-\mathbf{u})(\boldsymbol{\xi}-\mathbf{u}) : \nabla\mathbf{u}\right]/R \tag{9a}$$

$$\Re^{II} = -f^{eq}\left[(\boldsymbol{\xi}-\mathbf{u})(\boldsymbol{\xi}-\mathbf{u}) : \nabla\mathbf{u}\right]/R \tag{9b}$$

$$\Re^{III} = -f(\boldsymbol{\xi}-\mathbf{u}).\left[\partial_t\mathbf{u} + (\mathbf{u}.\nabla)\mathbf{u}\right]/R \tag{9c}$$

It should be mentioned that in the incompressible limit (which is the limit of small Mach number, $Ma \to 0$), $\Re^{II}$ and $\Re^{III}$ become negligible and hence $\Re = \Re^I$. In Eq. (7), Q is the

energy source term that features out of the physical situation within the participating fluid media. The macroscopic temperature can be obtained from the temperature DF g as: $\rho c_p T = \int g d\boldsymbol{\xi} + \int (\Re + Q) d\boldsymbol{\xi}$. Since two separate kinetic equations with corresponding DFs are used to describe the flow and thermal fields respectively, the kinematic viscosity and thermal diffusivity can be independently adjusted, which makes the model suitable for varying Prandtl number flows.

Eqs. (5) and (7) can now be represented by the following generic discrete-velocity form:

$$\partial_t \psi_i + \boldsymbol{\xi}_i \cdot \nabla \psi_i = -\left(\psi_i - \psi_i^{eq}\right) \Big/ \lambda + \Phi_i \tag{10}$$

where $\psi = f$ or g, $\lambda = \lambda_f$ or λ_g, $\Phi = F$ or $\Re + Q$ for the respective kinetic equations and $i \in \{1, b\}$ stands for the b base vectors of the underlying lattice type. Eq. (10) is subsequently integrated along its characteristic using the second order trapezoidal rule (He et al., 1998) to yield the discrete evolution equation:

$$\begin{aligned} &\psi_i(\mathbf{x} + \boldsymbol{\xi}_i \delta t, \boldsymbol{\xi}_i, t + \delta t) - \psi_i(\mathbf{x}, \boldsymbol{\xi}_i, t) = -\frac{\delta t}{2\lambda}\left[\psi_i(\mathbf{x} + \boldsymbol{\xi}_i \delta t, \boldsymbol{\xi}_i, t + \delta t) - \psi_i^{eq}(\mathbf{x} + \boldsymbol{\xi}_i \delta t, \boldsymbol{\xi}_i, t + \delta t)\right] \\ &-\frac{\delta t}{2\lambda}\left[\psi_i(\mathbf{x}, \boldsymbol{\xi}_i, t) - \psi_i^{eq}(\mathbf{x}, \boldsymbol{\xi}_i, t)\right] + \frac{\delta t}{2}\Phi_i(\mathbf{x} + \boldsymbol{\xi}_i \delta t, \boldsymbol{\xi}_i, t + \delta t) + \frac{\delta t}{2}\Phi_i(\mathbf{x}, \boldsymbol{\xi}_i, t) \end{aligned} \tag{11}$$

where δt denotes the time step. The forcing parameter and the discrete equilibrium DFs can be constructed as:

$$F_i = w_i \rho \left[\frac{\boldsymbol{\xi}_i - \mathbf{u}}{c_s^2} + \frac{(\boldsymbol{\xi}_i \cdot \mathbf{u})}{c_s^4}\boldsymbol{\xi}_i\right] \cdot \mathbf{F} \tag{12}$$

$$f_i^{eq} = w_i \rho \left[1 + \frac{(\boldsymbol{\xi}_i \cdot \mathbf{u})}{c_s^2} + \frac{\mathbf{uu} : (\boldsymbol{\xi}_i \boldsymbol{\xi}_i - c_s^2 \mathbf{I})}{2c_s^4}\right], \; g_i^{eq} = c_p T f_i^{eq} \tag{13}$$

Finally, the energy sources can be formulated as:

$$\Re_i = \Re_i^I = -T\left(f_i - f_i^{eq}\right)\frac{(\boldsymbol{\xi}_i - \mathbf{u})(\boldsymbol{\xi}_i - \mathbf{u}) : \nabla \mathbf{u}}{c_s^2}, \; Q_i = w_i \dot{q}\left[1 + \frac{(\boldsymbol{\xi}_i \cdot \mathbf{u})}{c_s^2}\right] \tag{14}$$

The weights w_i and the discrete velocities $\boldsymbol{\xi}_i$ correspond to the D2Q9 configuration (He et al., 1998) (refer to Fig. 1) as:

$$w_i = \begin{cases} 4/9 & i = 0 \\ 1/9 & i = 1,2,3,4 \\ 1/36 & i = 5,6,7,8 \end{cases} \tag{15}$$

$$\boldsymbol{\xi}_i = \begin{cases} \mathbf{0} & i = 0 \\ \left(\cos\left[(i-1)\pi/2\right], \sin\left[(i-1)\pi/2\right]\right)c & i = 1,2,3,4 \\ \sqrt{2}\left(\cos\left[(i-5)\pi/2 + \pi/4\right], \sin\left[(i-5)\pi/2 + \pi/4\right]\right)c & i = 5,6,7,8 \end{cases} \tag{16}$$

where $c\left(=\sqrt{3RT}\right)$ is the characteristic speed, and the sound speed of the model is chosen as $c_s=\sqrt{RT}=1/\sqrt{3}$.

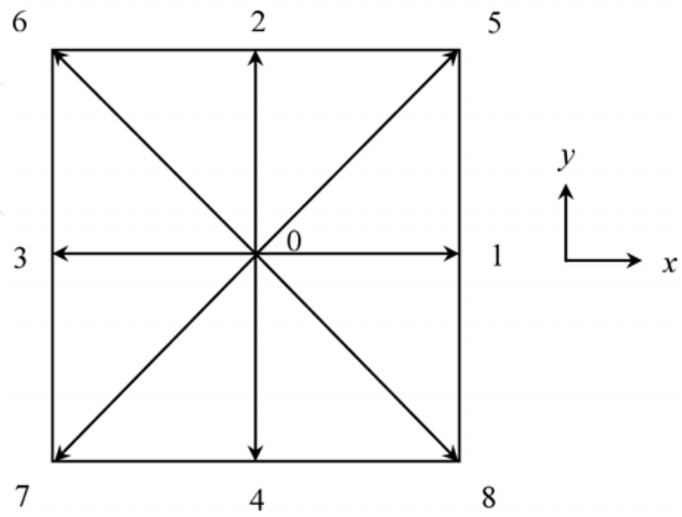

Fig. 1. Discretized 2D velocity space (D2Q9)

By using the Chapman-Enskog multiscale expansion, Eq. (11) correctly recovers the macroscopic conservation equations in the incompressible limit by setting the kinematic viscosity as $\nu=c_s^2\left(\lambda_f^*-0.5\right)\delta t$, where $\lambda_f^*=0.5+\left(\lambda_f-0.5\right)/\rho\left(\mathbf{x},t,T\right)$ is the modified relaxation time for the non-isothermal flows (Chatterjee & Chakraborty, 2006) with $\rho\left(\mathbf{x},t,T\right)=\sum_i f_i\left(\mathbf{x},t,T\right)$ being the local particle density and the thermal diffusivity as $\alpha=\kappa/\rho c_p=c_s^2\left(\lambda_g-0.5\right)\delta t$. Accordingly, the approach offers the possibility of varying the Prandtl number by adjusting the relaxation times of the respective kinetic equations as: $\mathrm{Pr}=\nu/\alpha=\left(\lambda_f^*-0.5\right)/\left(\lambda_g-0.5\right)$.

In order to avoid implicitness of Eq. (11), we further introduce (He et al., 1998) $\overline{\psi}_i=\psi_i+\frac{\delta t}{2\lambda}\left[\psi_i-\psi_i^{eq}\right]-\frac{\delta t}{2}\Phi_i$. Consequently, the discretized evolution equations for $\overline{\psi}_i$ become

$$\overline{\psi}_i\left(\mathbf{x}+\boldsymbol{\xi}_i\delta t,\boldsymbol{\xi}_i,t+\delta t\right)=\overline{\psi}_i\left(\mathbf{x},\boldsymbol{\xi}_i,t\right)-\frac{\delta t}{\left(\lambda+0.5\delta t\right)}\left[\overline{\psi}_i\left(\mathbf{x},\boldsymbol{\xi}_i,t\right)-\psi_i^{eq}\left(\mathbf{x},\boldsymbol{\xi}_i,t\right)\right]+\\+\frac{\lambda\delta t}{\left(\lambda+0.5\,\delta t\right)}\Phi_i\left(\mathbf{x},\boldsymbol{\xi}_i,t\right) \tag{17}$$

The macroscopic flow and thermal quantities are obtained from $\overline{f}_i$ and $\overline{g}_i$ as: $\rho=\sum_i\overline{f}_i$, $\rho\mathbf{u}=\sum_i\boldsymbol{\xi}_i\overline{f}_i+\left(\delta t/2\right)\rho\mathbf{F}$, $\rho c_pT=\sum_i\overline{g}_i+\left(\delta t/2\right)\sum_i\left(\Re_i+Q_i\right)$.

3. Numerical implementation

3.1 Enthalpy update

For accurate prediction of the liquid fraction, the latent enthalpy content of each computational cell needs to be updated according to the predicted macroscopic value of temperature each iteration within a time step. For that purpose, an enthalpy updating scheme in accordance with the formulation of Brent et al. (1988) is used, which is of the form, $[\Delta h]_{n+1} = [\Delta h]_n + \eta\left\{[h_s]_n - F^{-1}[\Delta h]_n\right\}$, where n is the iteration level characterizing the updation stage, h_s is the sensible enthalpy of the concerned cell, Δh is the latent heat contained by the cell, and η is a suitable relaxation factor to smoothen convergence. In the above formulation, $F^{-1}[\Delta h]$ is an appropriate mathematical function, which needs to be constituted in consistency with microscopic phase change considerations. A detailed guideline in this regard can be found in Chakraborty & Dutta (2001). For the case of pure material phase change an appropriate choice of the function can be $F^{-1}[\Delta h] = c_p T_m$, where T_m is the equilibrium freezing temperature in presence of a flat interface. With the updated Δh, nodal values of sensible heat, and hence the temperature can be obtained as:

$$[h_s]_{n+1} = [h]_{n+1} - [\Delta h]_{n+1} = c_p [T]_{n+1} \tag{18}$$

3.2 Boundary conditions

A no-slip hydrodynamic boundary condition and both Neumann and Dirichlet type thermal boundary conditions at the walls can be used. The non-equilibrium extrapolation method (Guo et al., 2002), which has a good numerical accuracy and stability, can be adopted to implement the above mentioned boundary conditions in the LB framework. According to this method, the non-equilibrium part of the DF at a boundary node can be well approximated by the same at the nearest neighboring node in the fluid region along the discrete velocity. As an example, if $\mathbf{x}_b$ represents a boundary node and $\mathbf{x}_f$ its nearest neighboring fluid node, then $f_i^{neq}(\mathbf{x}_b) = f_i^{neq}(\mathbf{x}_f)$ and $g_i^{neq}(\mathbf{x}_b) = g_i^{neq}(\mathbf{x}_f)$, and the total DF at $\mathbf{x}_b$ can be given as:

$$f_i(\mathbf{x}_b) = f_i^{eq}\left[\rho^*(\mathbf{x}_b), \mathbf{u}^*(\mathbf{x}_b)\right] + \left[f_i(\mathbf{x}_f) - f_i^{eq}(\mathbf{x}_f)\right] \tag{19}$$

$$g_i(\mathbf{x}_b) = g_i^{eq}\left[\rho^*(\mathbf{x}_b), \mathbf{u}^*(\mathbf{x}_b), T^*(\mathbf{x}_b)\right] + \left[g_i(\mathbf{x}_f) - g_i^{eq}(\mathbf{x}_f)\right] \tag{20}$$

where the equilibrium part of the DF is determined by imposing the macroscopic boundary conditions through the auxiliary density ρ^*, velocity $\mathbf{u}^*$ or temperature T^*. For example, if velocity $\mathbf{u}(\mathbf{x}_b)$ and temperature $T(\mathbf{x}_b)$ are known but $\rho(\mathbf{x}_b)$ is unknown, we may use $\rho^*(\mathbf{x}_b) = \rho(\mathbf{x}_f)$ or $\rho^*(\mathbf{x}_b) = 2\rho(\mathbf{x}_f) - \rho(\mathbf{x}_{ff})$ with $\mathbf{x}_{ff}$ as the next neighboring fluid node of $\mathbf{x}_b$ in the same direction, and $\mathbf{u}^*(\mathbf{x}_b) = \mathbf{u}(\mathbf{x}_b)$, $T^*(\mathbf{x}_b) = T(\mathbf{x}_b)$. $\mathbf{u}^*$ and T^* are specified according to the given boundary conditions for $\mathbf{u}$ and T.

A Neumann boundary condition can be implemented by transferring it to the Dirichlet type boundary condition by using a conventional second order finite difference approximation to obtain the boundary temperatures (Shu et al., 2002), in an iterated manner. Regarding interface conditions, it is apparent that the solid/liquid interface in phase change problems

acts as a wall, and the same needs to be treated appropriately. However, according to the enthalpy-porosity formulation, one does not need to track the interface separately and impose hydrodynamic or thermal boundary conditions on the same, since the interface comes out as a natural outcome of the solution procedure itself.

3.3 Numerical scheme

The simulation starts with the prescribed initial values of the temperature $T(\mathbf{x},0)$, velocity $\mathbf{u}(\mathbf{x},0)$ and liquid-fraction $f_l(\mathbf{x},0)$. The sensible enthalpy $h_s(\mathbf{x},0)$ and latent enthalpy $\Delta h(\mathbf{x},0)$ values are obtained from the prescribed initial conditions. Thereafter, the initial DFs $\overline{f}_i(\mathbf{x},0)$ and $\overline{g}_i(\mathbf{x},0)$ are computed using one term in their respective Knudsen expansions, i.e., $\overline{f}_i(\mathbf{x},0) = f_i^{eq}(\mathbf{x},0)$ and $\overline{g}_i(\mathbf{x},0) = g_i^{eq}(\mathbf{x},0)$. Distribution functions are then evolved according to Eq. (17). The overall solution algorithm is as follows:

i. Read the geometry
ii. Set initial conditions $\mathbf{u}(\mathbf{x},0)$, $T(\mathbf{x},0)$ and $f_l(\mathbf{x},0)$
iii. Calculate sensible and latent enthalpy $h_s(\mathbf{x},0)$ and $\Delta h(\mathbf{x},0)$
iv. Calculate initial equilibrium DFs $f_i^{eq}(\mathbf{x},0)$ and $g_i^{eq}(\mathbf{x},0)$
v. Set the initial DFs $\overline{f}_i(\mathbf{x},0) = f_i^{eq}(\mathbf{x},0)$ and $\overline{g}_i(\mathbf{x},0) = g_i^{eq}(\mathbf{x},0)$

Time loop
{
1. Impose boundary conditions
2. Propagate fluid particles (Streaming)
3. Calculate equilibrium DFs f_i^{eq} and g_i^{eq}
4. Calculate relaxation
5. Obtain velocity, temperature and liquid fraction fields
6. Update nodal enthalpy
7. Go back to step 1 until convergence

}
vi. Obtain macroscopic variables

The convergence is declared if the following criterion is satisfied:

$$\min\left(\left|\frac{\mathbf{u}^{n+1}-\mathbf{u}^{n}}{\mathbf{u}^{n}}\right|,\left|\frac{T^{n+1}-T^{n}}{T^{n}}\right|,\left|\frac{\Delta h^{n+1}-\Delta h^{n}}{\Delta h^{n}}\right|\right) \le 10^{-8} \tag{21}$$

The relaxation parameters should lie in the range $0.5 < \lambda_i < 1$, $i = f, g$ such that positive distribution functions can be obtained close to the local equilibrium, thereby ensuring non-linear stability of the numerical scheme (Higuera et al., 1989). It should be emphasized here that a rigorous, exact, theoretical analysis of nonlinear stability of the scheme is impossible, for it would amount to solving the lattice Boltzmann equations (LBE) itself. However, a number of general guiding criteria prove fairly useful. One of these criteria is the conservativeness of the scheme. The streaming operators in the LBE are perfectly conservative and the collision operators are also conservative. This makes the method an

exactly conserving numerical scheme which automatically protect against numerical blow-ups in the actual simulation (Chatterjee, 2009).

4. Case studies

We present here some case studies such as 1-D and 2-D solidification/melting problems for which analytical solutions are available and some other benchmark problems in melting and solidification.

4.1 1-D directional solidification

A one-dimensional (1-D) directional solidification problem is solved for which analytical solution is available. The schematic of the problem is shown in Fig. 2. Initially, the material is kept in a molten state at a temperature T_i (= 1) higher than the melting point T_m (= 0.5). Heat is removed from the left at a temperature T_0, which is scaled to be zero. The one-dimensional infinite domain is simulated by a finite domain (considering a domain extent of 4). The analytical solutions for the interface position $\xi(t)$, the solid (T_s) and liquid (T_l) temperatures are given by (Voller, 1997; Palle & Dantzig, 1996):

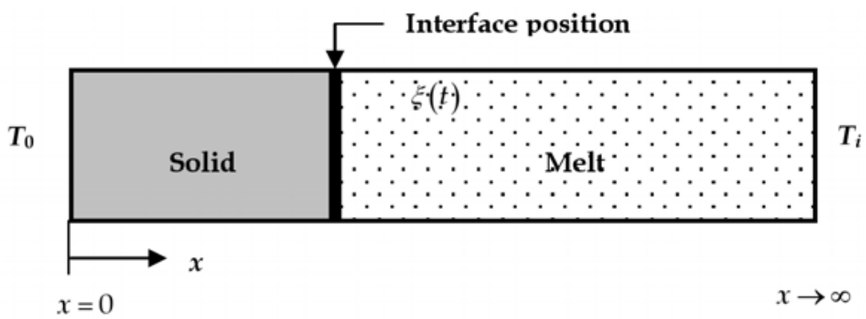

Fig. 2. Schematic of the one-dimensional solidification problem (Chatterjee, 2010)

$$\xi(t)=2\gamma\sqrt{t}\ ,\ T_s=\frac{T_m}{erf(\gamma)}erf\left(x/\sqrt{4t}\right),\ T_l=1+\frac{T_m-1}{erf(\gamma)}erf\left(x/\sqrt{4t}\right) \tag{22}$$

where γ is a constant and can be obtained implicitly from the transcendental equation,

$$T_m=erf(\gamma)\left(1+\frac{\sqrt{\pi}}{St}\gamma\exp\left(\gamma^2\right)erfc(\gamma)\right) \tag{23}$$

Numerical simulation is performed by considering 40 uniform lattices in total in the computational range from x = 0 to 4. The dimensionless time, position and temperature are defined as $\overline{t}=\alpha t/Y^2$, $\overline{x}=x/Y$ and $\overline{T}=(T-T_0)/(T_i-T_0)$ respectively and the numerical value of Y is set as unity. The calculated isotherms at different times and the interface positions at different Stefan numbers ($St=c_p\Delta T/L$, where $\Delta T=T_i-T_0$) are shown in Fig. 3 (a, b). An excellent agreement is found between the present simulation and the analytical solution which in turn demonstrates the effectiveness of the proposed method.

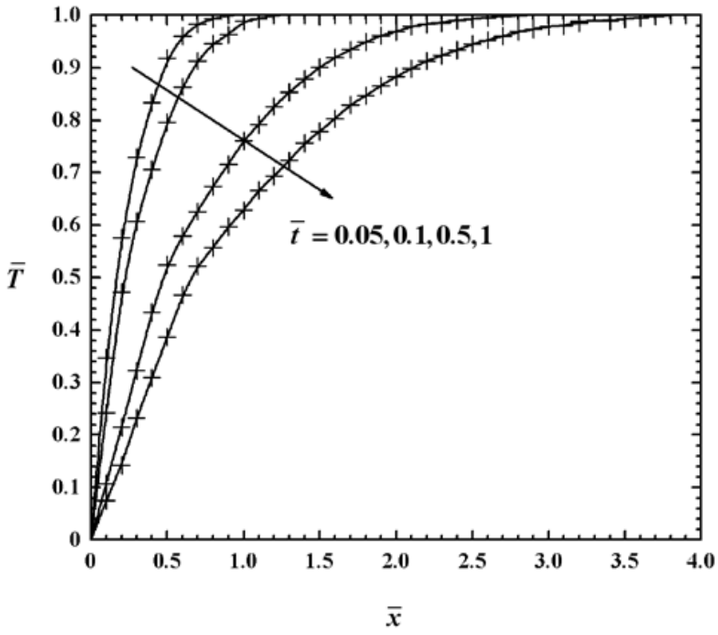

(a)

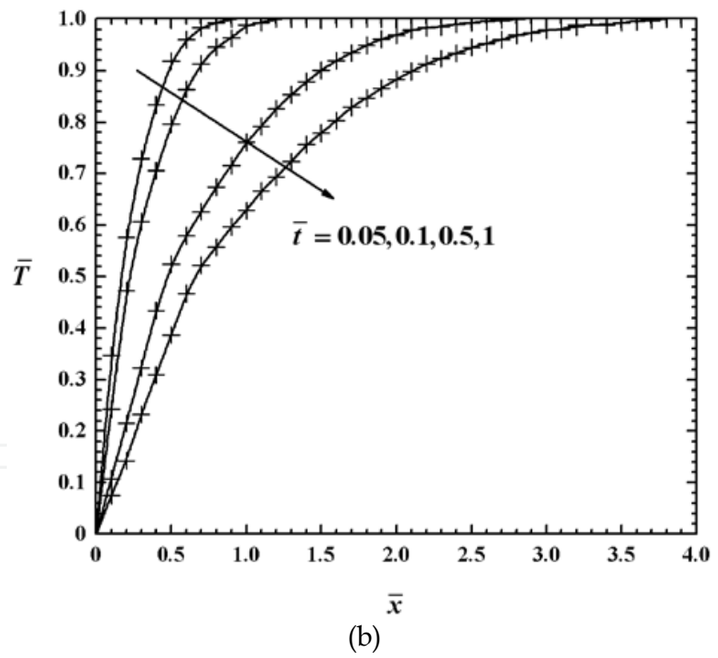

(b)

Fig. 3. Comparison of calculated (symbol) (a) isotherms for St = 1 at different times, and (b) interface position at different Stefan numbers with analytical solutions (solid lines) for the one-dimensional solidification problem (Chatterjee, 2010)

4.2 2-D solidification problem

A two-dimensional (2-D) solidification problem for which analytical (Rathjen & Jiji, 1971) and numerical (LB) (Jiaung et al., 2001; Lin & Chen, 1997) solutions are available in the

literature is now presented. Fig. 4 shows the schematic diagram of the problem with the boundary conditions. The material is kept initially at a uniform temperature T_i which is higher than or equal to the melting temperature $T_{m.}$ The left (x = 0) and bottom (y = 0) boundaries are lowered to some fixed temperature $T_0 \left(< T_m \right)$ and consequently, solidification begins from these surfaces and proceeds into the material. Setting the scaled temperatures $T_i = 0.3$, $T_0 = -1$ and $T_m = 0$ as considered in Jiaung et al. (2001) and Rathjen & Jiji (1971) and assuming constant material properties, we obtain the LB simulation results following the proposed methodology. Fig. 5a and b depict the interface position and isotherms respectively at a normalized time $\bar{t} = 0.25$ and $St = c_p \left(T_m - T_0 \right) / L = 4$. The interval between the isotherm lines is 0.2 units (dimensionless). The agreement with the available analytical and numerical results is quiet satisfactory. This in turn demonstrates the accuracy and usefulness of the proposed method.

4.3 Melting of pure gallium

Melting of pure gallium in a rectangular cavity is a standard benchmark problem for validation of phase change modeling strategies, since reliable experiments in this regard (particularly, flow visualization and temperature measurements) have been well-documented in the literature (Gau & Viskanta, 1986). Brent et al. (1988) solved this problem numerically with a first order finite volume scheme, coupled with an enthalpy-porosity approach, and observed an unicellular flow pattern, in consistency with experimental findings reported in Gau & Viskanta (1986), whereas Dantzig (1989) obtained a multicellular flow pattern, by employing a second order finite element enthalpy-porosity model. Miller et al. (2001), again, obtained a multicellular flow patterns while simulating the above problem,

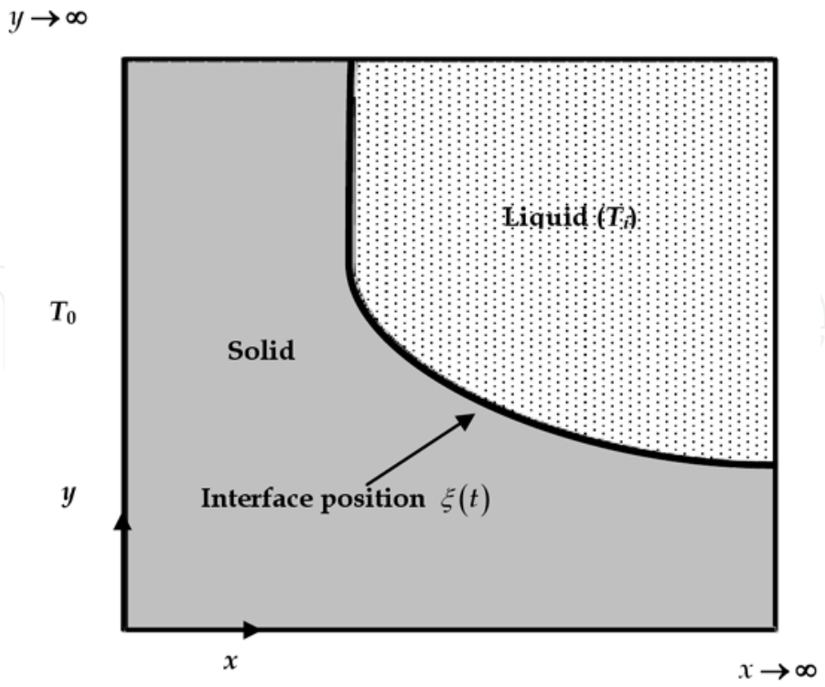

Fig. 4. Schematic of the two-dimensional solidification problem (Chatterjee, 2010)

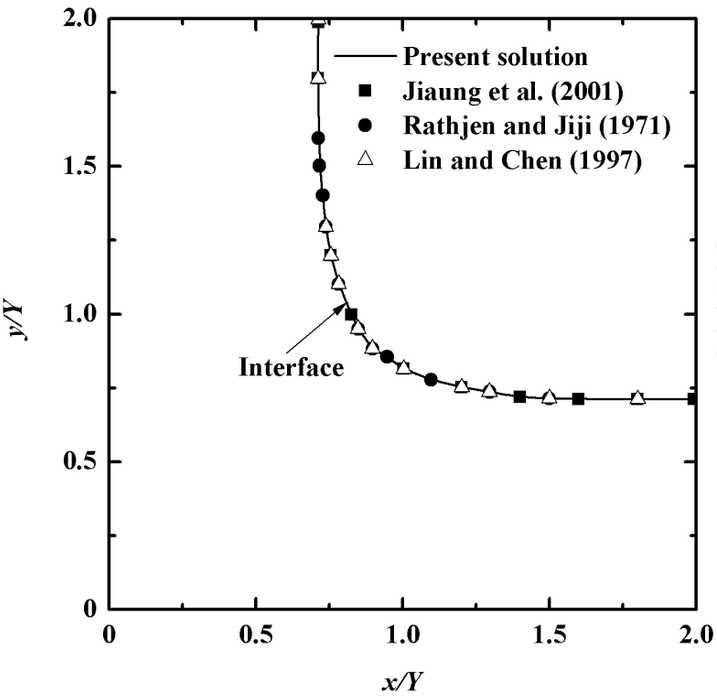

(a)

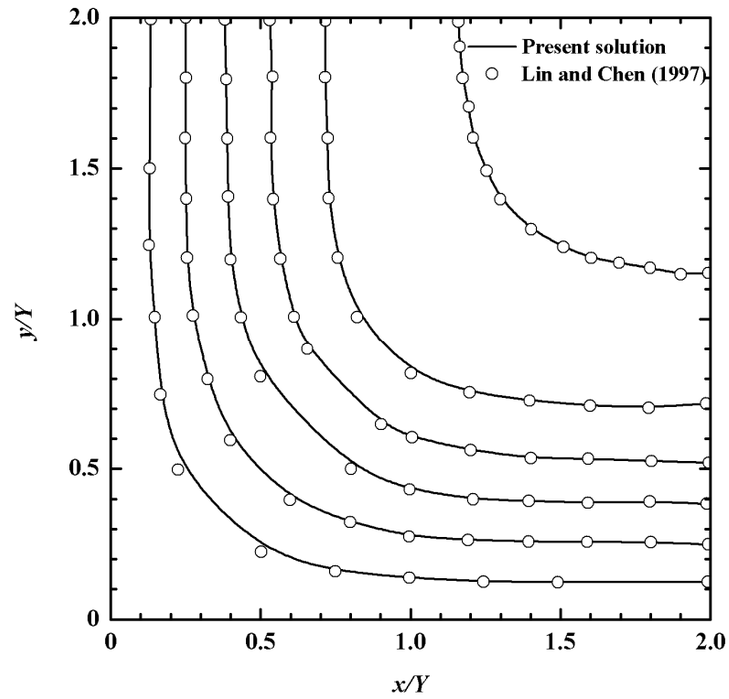

(b)

Fig. 5. Comparison of (a) interface position and (b) isotherm at $\overline{t} = 0.25$ for the two-dimensional solidification problem (Chatterjee, 2010)

by employing a LB model in conjunction with the phase field method. In all the above cases, nature of the flow field was observed to be extremely sensitive to problem data employed for numerical simulations. Here, simulation results (Chakraborty & Chatterjee, 2007) are shown with the same set of physical and geometrical parameters, as adopted in Brent et al. (1988). The study essentially examines a two-dimensional melting of pure gallium in a rectangular cavity, initially kept at its melting temperature, with the top and bottom walls maintained as insulated. Melting initiates from the left wall with a small thermal disturbance, and continues to propagate towards the right. The characteristic physical parameters are as follows: Prandtl number (Pr) = 0.0216, Stefan number (St) = 0.039 and Raleigh number (Ra) = 6×10^5. Numerical simulations are performed with a (56 × 40) uniform grid system, keeping the aspect ratio 1.4 in a 9 speed square lattice (D2Q9) over 6×10^5 time steps (corresponding to 1 min of physical time). The results show excellent agreements with the findings of Brent et al. (1988). For a visual appreciation of flow behavior during the melting process, Fig. 6 is plotted, which shows the streamlines and melt front location at time instants of 6, 10 and 19 min, respectively. The melting front remains virtually planar at initial times, as the natural convection field begins to develop. Subsequently, the natural convection intensifies enough to have a pronounced influence on overall energy transport in front of the heated wall. Morphology of the melt front is subsequently dictated by the fact that fluid rising at the heated wall travels across the cavity and impinges on the upper section of the solid front, thereby resulting in this area to melt back beyond the mean position of the front. After 19 min, the shape of the melting front is governed primarily by advection. Overall, a nice agreement can be seen between numerically obtained melt front positions reported in a benchmark study executed by Brent et al. (1988) and the present simulation. Slight discrepancies between the computed results

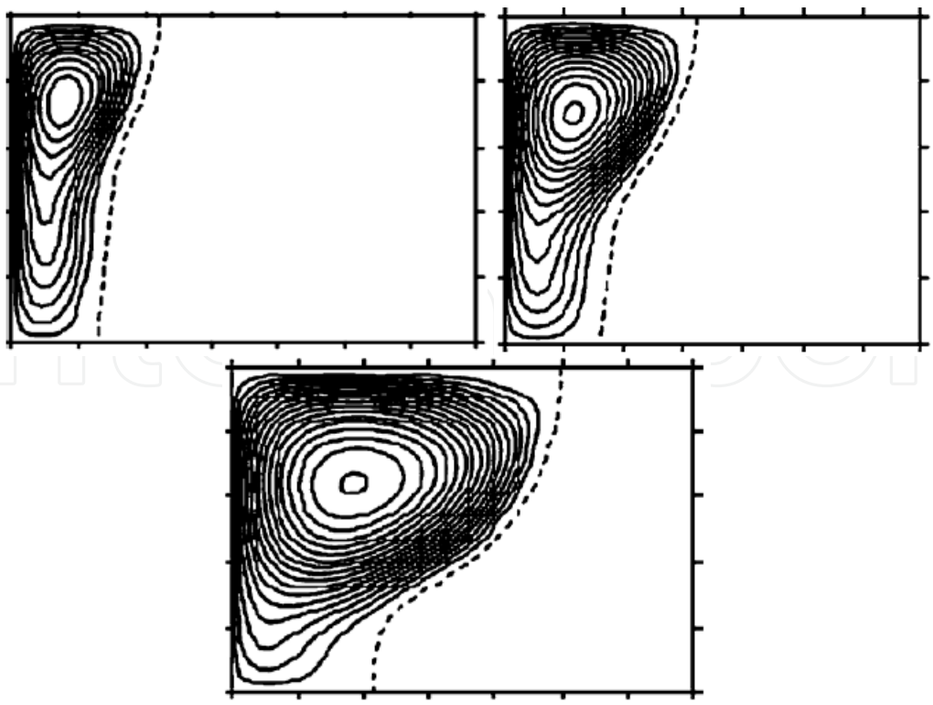

Fig. 6. Melting of pure gallium in a rectangular cavity (Chakraborty & Chatterjee, 2007)

(both in benchmark numerical work reported earlier and the present computations) and observed experimental findings (Gau & Viskanta, 1986) can be attributed to three-dimensional effects in experimental apparatus to determine front locations, experimental uncertainties and variations in thermo-fluid properties. However, from a comparison of the calculated and experimental (Gau & Viskanta, 1986) melt fronts at different times (refer to Fig. 7), it is found that both the qualitative behavior and actual morphology of the experimental melt fronts are realistically manifested in the present numerical simulation.

4.4 Bridgman crystal growth

Results are presented for simulation of transport processes in a macroscopic solidification problem such as the Bridgman crystal growth in a square crucible (Chatterjee, 2010). The Bridgman crystal growth is a popular process for growing compound semiconductor crystals and this problem has been solved extensively as a benchmark problem. The typical problem domain along with the boundary condition is shown schematically in Fig. 8. Initially, the material is kept in a molten state at a temperature T_i (= 1) higher than the melting point T_m. Since initially there is no thermal gradient, consequently, there is no convection. At $t = 0^+$, the left, right and the bottom walls are set to the temperature T_0, which is scaled to be zero, while the top wall is assumed to be insulated. This will lead to a new phase formation (solidification) at the walls with simultaneous melt convection. The characteristic physical parameters (arbitrary choice) for the problem are the Prandtl number Pr = 1, Stefan number St = 1 and Raleigh number $Ra = g_a \beta \Delta T A^3 / (\nu \alpha) = 10^5$, with A being

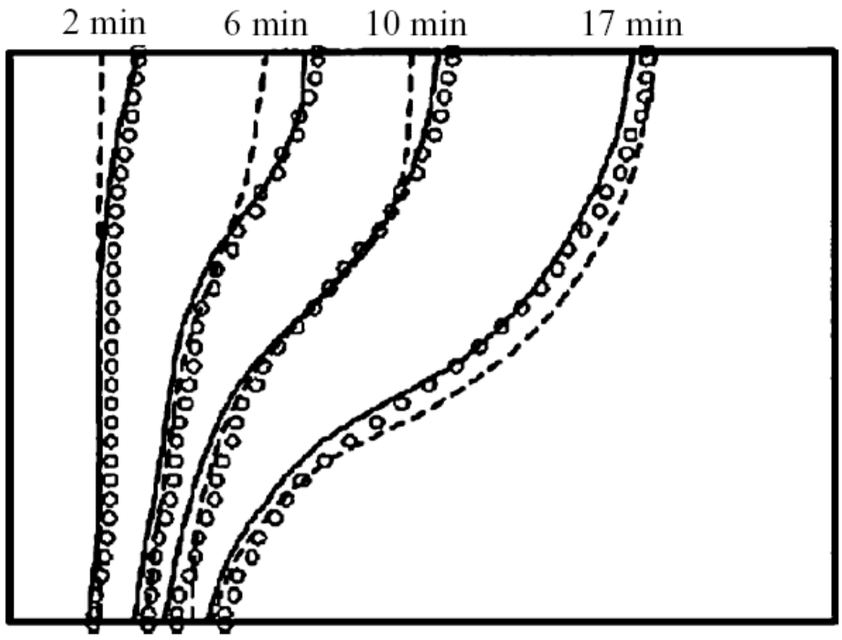

Fig. 7. Melting of pure gallium in a rectangular cavity: comparisons of the interfacial locations as obtained from the LB model (circles) with the corresponding experimental (Gau & Viskanta, 1986) results (dotted line) and continuum based numerical simulation (Brent et al., 1988) predictions (solid line) (Chakraborty & Chatterjee, 2007)

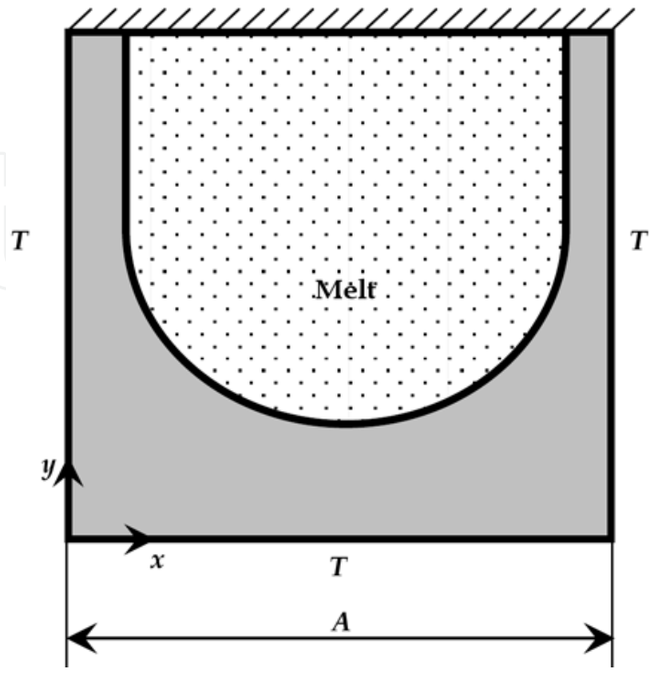

Fig. 8. Schematic of the Bridgman crystal growth in a square crucible (Chatterjee, 2010)

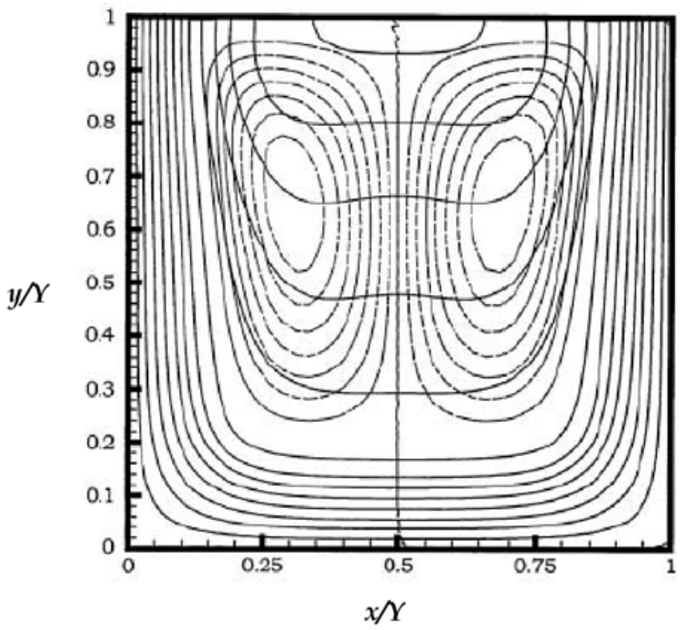

Fig. 9. Isotherm (continuous line) and flow pattern (dashed lines) at $\bar{t} = 0.25$ for the Bridgman crystal growth process (Chatterjee, 2010)

the characteristic dimension of the simulation domain. Numerical simulations are performed on a (80 × 80) uniform grid systems with an aspect ratio of 1, in a 9 speed square lattice (D2Q9) over 6×10^5 time steps corresponding to 1 min of physical time. For a visual appreciation of the overall evolution of the transport quantities in this case, Fig. 9 is plotted, which shows the representative flow pattern and isotherms at a normalized time instant of $\bar{t} = 0.05$. The interval between the contour lines is 0.05 units (dimensionless). Larger isotherm spacing is observed in the melt which is a consequence of the heat of fusion released from the melt as well as a subsequent convection effect. The isotherms are normal to the top surface since the top surface is an adiabatic wall. Two counter rotating symmetric cells are observed in the flow pattern which is consistent with the flow physics. The melt convection will become weaker as the solidification progresses since there is very little space for convection. Also the thermal gradient will become small at this juncture. The calculation continues until the melt completely disappears and the temperature of the entire domain eventually reaches T_0.

In order to demonstrate the capability of the proposed method in capturing the interfacial region without further grid refinement as normally required for the phase field based method or any other adaptive methods, Fig. 10 is plotted in which the comparison of the isotherm obtained from the present simulation for the Bridgman crystal growth and from an adaptive finite volume method (Lan et al., 2002) is shown. Virtually there is no deviation of

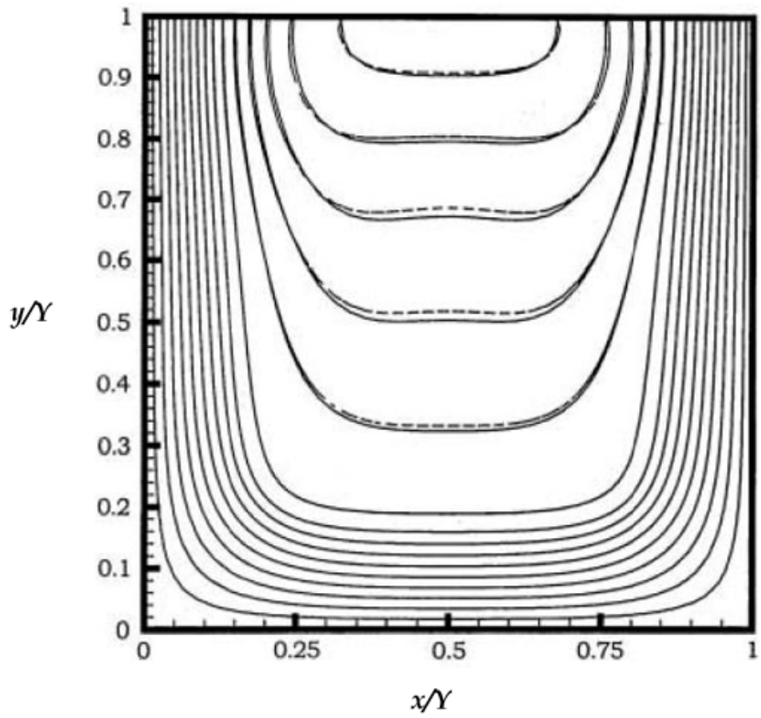

Fig. 10. Comparison of isotherm from the present calculation (solid lines) and from an adaptive finite volume method (dashed lines) (Lan et al., 2002) (Chatterjee, 2010)

the calculated isotherm form that obtained from the adaptive finite volume method (Lan et al., 2002) has been observed. This proves that the present method is quiet capable of capturing the interfacial region without further grid resolution.

4.5 Crystal growth during solidification

In this section, the problem of crystal growth during solidification of an undercooled melt is discussed (Chatterjee & Chakraborty, 2006). Special care is taken to model the effects of curvature undercooling, anisotropy of surface energy at the interface and the influence of thermal noise, borrowing principles from cellular automaton based dendritic growth models (Sasikumar & Sreenivasan, 1994; Sasikumar & Jacob, 1996), in the framework of a generalized enthalpy updating scheme adopted here. Numerical experiments are performed to study the effect of melt convection on equiaxed dendrite growth. Since flow due to natural convection (present in a macroscopic domain) can be simulated as a forced flow over microscopic scales, a uniform flow is introduced through one side of the computational domain, and its effect on dendrite growth morphology is investigated. Computations are carried out in a square domain (50 × 50 uniform grid-system) containing initially a seed crystal at the center, while the remaining portion of the domain is filled with a supercooled melt. The physical parameters come from the following normalization of length (W) and time (τ) units: $W = \sqrt{2}\delta$ and $\tau = 2\delta^2 / \mu_k \varphi_g$, where δ is the interfacial length scale (typically O (10^{-9} m)), μ_k is a kinetic coefficient (typically O (10^{-1} m/s.K)) and φ_g is the Gibbs-Thompson coefficient (typically O (10^{-7} m.K)). Exact values of the above parameters have been taken from Beckermann et al. (1999). The degree of undercooling corresponds to 0.515 K. Fig. 11 demonstrates the computed evolution of dendritic arms under the above conditions. In absence of fluid flow, the dendrite arms grow in an identical manner

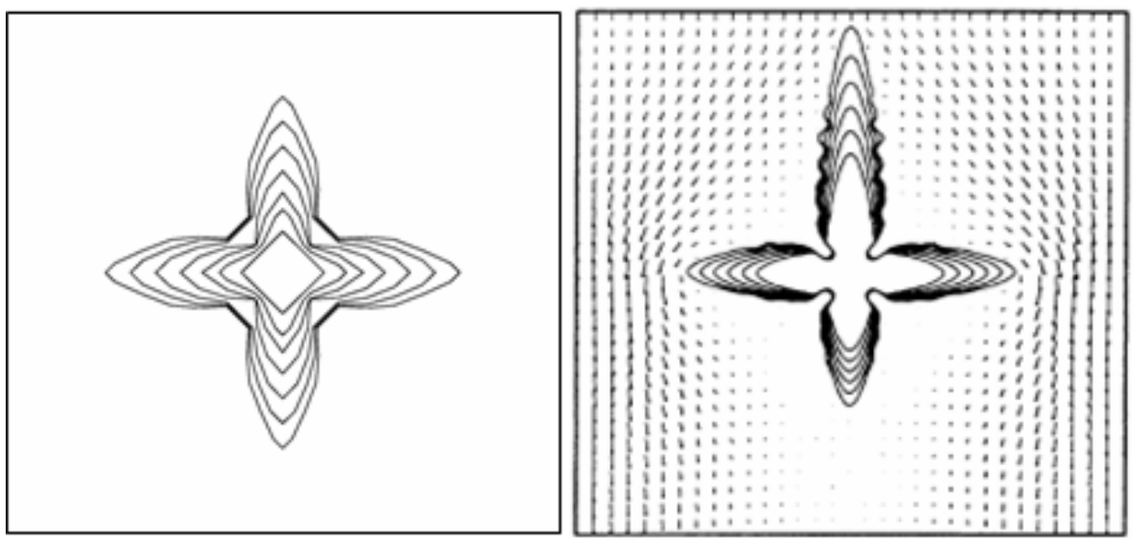

(a) (b)

Fig. 11. Effect of fluid flow on evolution of dendrite (Pr = 0.002) (0.4, 0.8, 1.2, 1.6, 2, 2.4 and 2.8 s) (a) with only diffusion (b) in presence of fluid flow. The interval between solid fraction contour lines is 0.05 units (dimensionless) (Chatterjee & Chakraborty, 2006)

(Fig. 11a), simply because of isotropic heat extraction through all four boundaries. Fig. 11(b) illustrates the effect of convection on the above dendritic growth. In the upstream side (top), convection opposes heat diffusion, which subsequently reduces the thermal boundary layer thickness and increases local temperature gradients, eventually, leading to a faster growth of the upper dendritic arm. Evolution of the downstream arm (bottom), on the other hand, is relatively retarded, for identical reasons.

For a more comprehensive validation of the quantitative capabilities of the present LB model to simulate dendritic growth in presence of fluid flow, results predicted by the present model are compared with those reported in Beckermann et al. (1999), and a visual appreciation of the same is depicted in Fig. 12. It is revealed from Fig. 12 that the solid fraction contours and isotherms based on the present model match excellently with the dendritic envelopes depicted in Beckermann et al. (1999). These results, further, indicate excellent convergence properties of the present LB based method, over a wide range of Reynolds and Prandtl numbers.

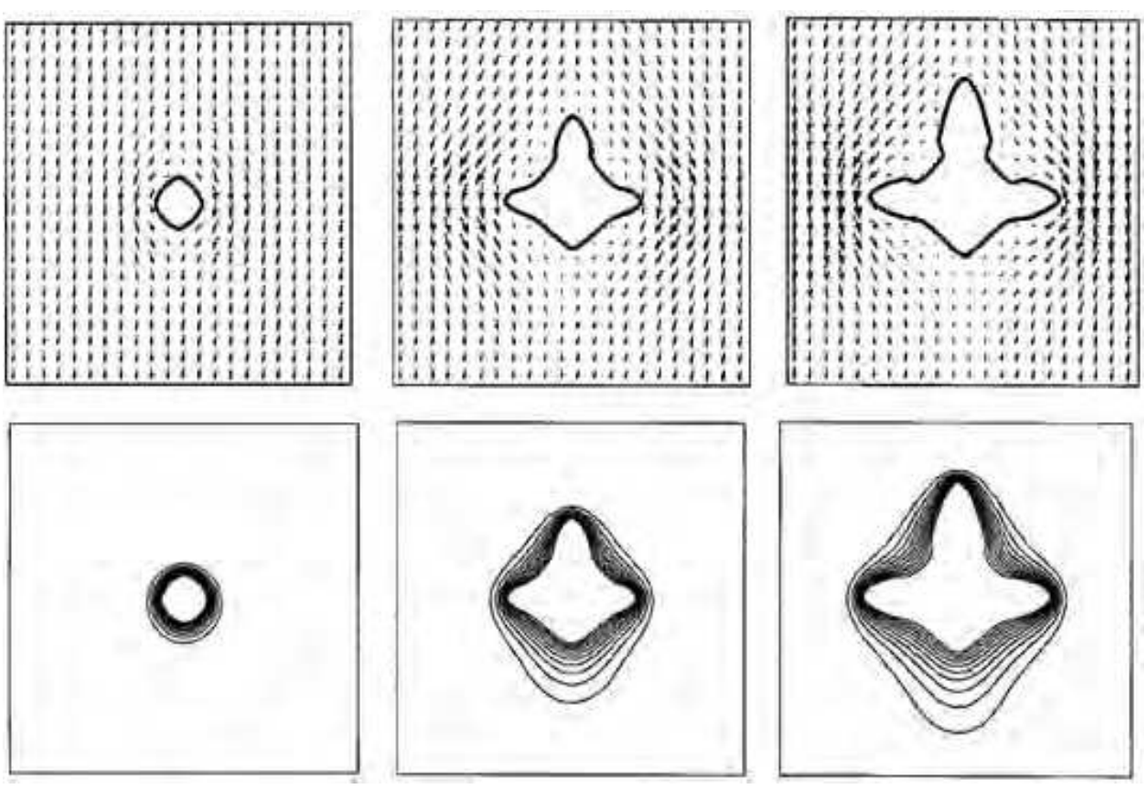

Fig. 12. LB Simulation of dendritic growth by employing problem data reported in Beckermann *et al*. (1999), solid fraction contour with velocity vectors (top panel) and isotherms (bottom panel), a) t = 2 s (b) t = 8 s (c) t = 12 s. The interval between isotherms is 0.05 units (dimensionless) (Chatterjee & Chakraborty, 2006)

5. Summary

This chapter briefly summarizes the development of a passive scalar based thermal LB model to simulate the transport processes during melting/freezing of pure substances. The model incorporates the macroscopic phase changing aspects in an elegant and straightforward manner into the LB equations. Although the model is developed for two-dimensional phase change problems, it can be easily extended to three-dimension. These features make the model attractive for simulating generalized convection-diffusion melting/solidification problems. Because of its inherent simplicity in implementation, stability, accuracy, as well as its parallel nature, the proposed method might be a potentially powerful tool for solving complex phase change problems in physics and engineering, characterized by complicated interfacial topologies. Compared with the phase field based LB models, the present scheme is much simpler to implement, since extremely refined meshes are not required here to resolve a minimum length scale over the interfacial regions. Although a finer mesh would definitely results in a better-resolved interface and a more accurate capturing of gradients of field variables, the mesh size for the present model merely plays the role of a synthetic microscope to visualize topological features of the interface morphology.

6. Acknowledgment

The author gratefully acknowledge Dr. Bittagopal Mondal (Scientist, Simulation & Modeling Laboratory, CSIR-Central Mechanical Engineering Research Institute, India) for reading the chapter and suggesting some modifications/corrections.

7. References

Askar, H.G. (1987). The front tracking scheme for the one-dimensional freezing problem. *International Journal for Numerical Methods in Engineering*, Vol. 24, pp. 859-869

Barrios, G.; Rechtman, R.; Rojas, J. & Tovar, R. (2005). The lattice Boltzmann equation for natural convection in a two-dimensional cavity with a partially heated wall. *Journal of Fluid Mechanics*, Vol. 522, pp. 91-100.

Beckermann, C.; Diepers, H.-J.; Steinbach, I.; Karma, A. & Tong, X. (1999). Modeling melt convection in phase-field simulations of solidification. *Journal of Computational Physics*, Vol. 154, pp. 468-496

Bhatnagar, P.L.; Gross, E.P. & Krook, M. (1954). A model for collision processes in charged and neutral one-component system. *Physical Review*, Vol. 94, pp. 511-525

Brent, A.D.; Voller, V.R. & Reid, K. (1988). Enthalpy-porosity technique for modeling convection–diffusion phase change: application to the melting of a pure metal. *Numerical Heat Transfer*, Vol. 13, pp. 297-318

Chakraborty, S. & Chatterjee, D. (2007). An enthalpy-based hybrid lattice-Boltzmann method for modelling solid–liquid phase transition in the presence of convective transport. *Journal of Fluid Mechanics*, Vol. 592, pp. 155-175

Chakraborty, S. & Dutta, P. (2001). A generalized formulation for evaluation of latent heat functions in enthalpy-based macroscopic models for convection–diffusion phase change process. *Metallurgical Transactions B*, Vol. 32, pp. 562-564

Chatterjee, D. & Chakraborty, S. (2005). An enthalpy-based lattice Boltzmann model for diffusion dominated solid–liquid phase transformation. *Physics Letters A*, Vol. 341, pp. 320-330

Chatterjee, D. & Chakraborty, S. (2006). A hybrid lattice Boltzmann model for solid–liquid phase transition in presence of fluid flow. *Physics Letters A*, vol. 351, pp. 359-367

Chatterjee, D. & Chakraborty, S. (2008). An enthalpy-source based lattice Boltzmann model for conduction dominated phase change of pure substances. *International Journal of Thermal Sciences*, Vol. 47, pp. 552-559

Chatterjee, D. (2009). An enthalpy-based thermal lattice Boltzmann model for non-isothermal systems. *Euro physics Letters*, Vol. 86, pp. 14004

Chatterjee, D. (2010). Lattice Boltzmann simulation of incompressible transport phenomena in macroscopic solidification processes. *Numerical Heat Transfer B*, Vol. 58, pp. 55-72

Chen, S. & Doolen, G.D. (1998). Lattice Boltzmann method for fluid flows, *Annual Review of Fluid Mechanics*, Vol. 30, pp. 329-364

Comini, G.; Guidice, S.D. & Saro, O. (1990). A conservative algorithm for multidimensional conduction phase change. *International Journal for Numerical Methods in Engineering*, Vol. 30, pp. 697-709

Comini, G.; Guidice, S.D.; Lewis, R.W. & Zienkiewicz, O.C. (1974). Finite element solution of non-linear heat conduction problems with special reference to phase change. *International Journal for Numerical Methods in Engineering*, Vol. 8, pp. 613-624

Dalhuijsen, A.J. & Segal, A. (1986). Comparison of finite element techniques for solidification problems. *International Journal for Numerical Methods in Engineering*, Vol. 23, pp. 1807- 1829

Dantzig, J.A. (1989). Modeling liquid-solid phase changes with melt convection. *International Journal for Numerical Methods in Engineering*, Vol. 28, pp.1769-1785

De Fabritiis, G.; Mancini, A.; Mansutti, D. & Succi, S. (1998). Mesoscopic models of liquid/solid phase transitions. *International Journal of Modern Physics C*, Vol. 9, pp. 1405-1415

Dhatt, G.; Song, R. & Cheikh, A.N. (1989). Direct enthalpy method for solidification calculation, In: Gruber *et al*. (Ed.), *Proceedings of the Fifth International Symposium on Numerical Methods in Engineering*, pp. 487-494, Boston,

Ferreol, B. & Rothman, D.H. (1995). Lattice Boltzmann simulations of flow through fontainebleau sandstone. *Transport in Porous Media,* Vol. 20, pp. 3-20

Gau, C. & Viskanta, R. (1986). Melting and solidification of a pure metal on a vertical wall. *Journal of Heat Transfer*, Vol. 108, pp. 174-181

Gunstensen, A.K.; Rothman, D.H.; Zaleski, S. & Zanetti, G. (1991). A lattice-Boltzmann model of immiscible fluids, *Physical Review A,* Vol. 43, pp. 4320-4327

Guo, Z.; Zheng, C. & Shi, B. (2002). An extrapolation method for boundary conditions in lattice Boltzmann method. *Physics of Fluids*, Vol. 14, pp. 2007-2010

Harrowell, P.R. & Oxtoby, D.W. (1987). On the interaction between order and a moving interface: Dynamical disordering and anisotropic growth rates. *Journal of Chemical Physics*, Vol. 86, pp. 2932-2942

He, X.; Chen, S. & Doolen, G.D. (1998). A novel thermal model for the lattice Boltzmann method incompressible limit. *Journal of Computational Physics*, Vol. 146, pp. 282-300

Higuera, F.J.; Succi, S. & Benzi, R. (1989). Lattice gas-dynamics with enhanced collisions. *Euro physics Letters*, Vol. 9, pp. 345-349

Huber, C.; Parmigiani, A.; Chopard, B.; Manga, M. & Bachmann, O. (2008). Lattice Boltzmann model for melting with natural convection. *International Journal of Heat and Fluid Flow*, Vol. 29, pp. 1469-1480

Hu, H. & Argyropoulos, S.A. (1996). Mathematical modeling of solidification and melting: a review. *Modeling Simulation Material Science Engineering*, Vol. 4, pp. 371–396

Jiaung, W.-S.; Ho, J.-R. & Kuo, C.-P. (2001). Lattice-Boltzmann method for the heat conduction problem with phase change. *Numerical Heat Transfer B*, Vol. 39, pp. 167-187

Kendon, V.M.; Cates, M.E.; Pagonabarraga, I.; Desplat, J.-C. & Bladon, P. (2001). Inertial effects in three-dimensional spinodal decomposition of a symmetric binary fluid mixture: a lattice Boltzmann study. *Journal of Fluid Mechanics*, Vol. 440, pp. 147-203

Khachaturyan, A.G. (1996). Long-range order parameter in field model of solidification. *Philosophical Magazine A*, Vol. 74, pp. 3-14

Kim, Y-T.; Provatas, N.; Goldenfeld, N. & Dantzig, J.A. (1999). Universal dynamics of phase-field models for dendritic growth. *Physical Review E*, Vol. 59, pp. R2546-R2549

Lan, C.W.; Liu, C.C. & Hsu, C.M. (2002). An Adaptive Finite Volume Method for Incompressible Heat Flow Problems in Solidification. *Journal of Computational Physics*, Vol. 178, pp. 464-497

Lin, J.-Y. & Chen, H.-T. (1997). Hybrid Numerical Scheme for Nonlinear Two-Dimensional Phase-change Problems with the Irregular Geometry. *Heat and Mass Transfer*, Vol. 33, pp. 51-58

Medvedev, D. & Kassner, K. (2005). Lattice Boltzmann scheme for crystal growth in external flows. *Physical Review E*, Vol. 72, pp. 056703

Mikheev, L.V. & Chernov, A.A. (1991). Mobility of a diffuse simple crystal melt interface. *Journal of Crystal Growth*, Vol. 112, pp. 591-596

Miller, W. & Succi, S. (2002). A Lattice Boltzmann model for anisotropic crystal growth from melt. *Journal of Statistical Physics*, Vol. 107, pp. 173-186

Miller, W. (2001). The lattice Boltzmann method: a new tool for numerical simulation of the interaction of growth kinetics and melt flow. *Journal of Crystal Growth*, Vol. 230, pp. 263-269

Miller, W., & Schroder, W. (2001). Numerical modeling at the IKZ: an overview and outlook. *Journal of Crystal Growth*, Vol. 230, pp. 1-9

Miller, W.; Rasin, I. & Pimentel, F. (2004). Growth kinetics and melt convection. *Journal of Crystal Growth*, Vol. 266, pp. 283-288

Miller, W.; Succi, S. & Manutti, D. (2001). Lattice Boltzmann Model for Anisotropic Liquid-Solid Phase Transition. *Physical Review Letters*, Vol. 86, pp. 3578-3581

Morgan, K.; Lewis, R.W. & Zienkiewicz, O.C. (1978) An improved algorithm for heat conduction problems with phase change. *International Journal for Numerical Methods in Engineering*, Vol. 12, pp. 1191-1195

Palle, N. & Dantzig, J.A. (1996). An adaptive mesh refinement scheme for solidification problems. *Metallurgical Transactions A*, Vol. 27, pp. 707-718

Pham, Q.T. (1986). The use of lumped capacitance in the finite-element solution of heat conduction problems with phase change. *International Journal of Heat and Mass Transfer*, Vol. 29, pp. 285-291

Raj, R.; Prasad, A.; Parida, P.R. & Mishra, S.C. (2006). Analysis of solidification of a semitransparent planar layer using the lattice Boltzmann method and the discrete transfer method. *Numerical Heat Transfer A*, Vol. 49, pp. 279–299

Rasin, I.; Miller, W. & Succi, S. (2005). Phase-field lattice kinetic scheme for the numerical simulation of dendritic growth. *Physical Review E*, Vol. 72, pp. 066705

Rathjen, K.A. & Jiji, L.M. (1971). Heat Conduction with Melting or Freezing in a Corner. *Journal of Heat Transfer*, Vol. 93, pp. 101-109

Roose, J. & Storrer, O. (1984). Modelization of phase changes by fictitious heat flow. *International Journal for Numerical Methods in Engineering*, Vol. 20, pp. 217-225

Rubinsky, B. & Cravahlo, E.G. (1981). A finite element method for the solution of one-dimensional phase change problems. *International Journal of Heat and Mass Transfer*, Vol. 24, pp. 1987-1989

Sankaranarayanan, K.; Shan, X.; Kevrekidis, I.G. & Sundaresan, S. (2002). Analysis of drag and virtual mass forces in bubbly suspensions using an implicit formulation of the lattice Boltzmann method. *Journal of Fluid Mechanics*, Vol. 452, pp. 61-96

Sasikumar, R. & Jacob, E. (1996). Simulation of side branch evolution in thermal dendritic grains. *Scripta Materialia*, Vol. 35, pp. 505-510

Sasikumar, R. & Sreenivasan, R. (1994). Two dimensional simulation of dendrite morphology. *Acta Metallurgica et Materialia*, Vol. 42, pp. 2381-2386

Shan, X. & Chen, H. (1993). Lattice Boltzmann model for simulating flows with multiple phase and components, *Physical Review E*, Vol. 47, pp. 1815-1819

Shi, Y., Zhao; T.S. & Guo, Z.L. (2004). Thermal lattice Bhatnagar-Gross-Krook model for flows with viscous heat dissipation in the incompressible limit. *Physical Review E*, Vol. 70, pp. 066310

Shu, C.; Peng, Y. & Chew, Y.T. (2002). Simulation of natural convection in a square cavity by Taylor series expansion and least square based lattice Boltzmann method. *International Journal of Modern Physics C*, Vol. 13, pp. 1399-1414

Tong, X.; Beckermann, C.; Karma, A. & Li, Q. (2001). Phase-field simulations of dendritic crystal growth in a forced flow. *Physical Review E*, Vol. 63, pp. 061601-(1-16)

Voller, V. & Cross, M. (1981). Accurate solutions of moving boundary problems using the enthalpy method. *International Journal of Heat and Mass Transfer*, Vol. 24, pp. 545-556

Voller, V. & Cross, M. (1983). An explicit numerical method to track a moving phase change front. *International Journal of Heat and Mass Transfer*, Vol. 26, pp. 147-150

Voller, V.; Swaminathan, C.R. & Thomas, B.G. (1990). Fixed grid techniques for phase change problems: a review. *International Journal for Numerical Methods in Engineering*, Vol. 30, pp. 875- 898

Voller, V.R. & Prakash, C. (1987). A fixed grid numerical modeling methodology for convection–diffusion mushy region phase change problems. *International Journal of Heat and Mass Transfer*, Vol. 30, pp. 1709-1719

Voller, V.R. (1997). A similarity solution for the solidification of multicomponent alloys. *International Journal of Heat and Mass Transfer*, Vol. 40, pp. 2869-2877

Weaver, J.A. & Viskanta, R. (1986). Freezing of liquid saturated porous media. *International Journal of Heat and Mass Transfer*, Vol. 33, pp. 2721-2734

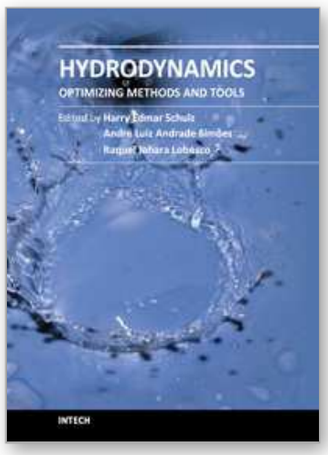

Hydrodynamics - Optimizing Methods and Tools
Edited by Prof. Harry Schulz

ISBN 978-953-307-712-3
Hard cover, 420 pages
Publisher InTech
Published online 26, October, 2011
Published in print edition October, 2011

The constant evolution of the calculation capacity of the modern computers implies in a permanent effort to adjust the existing numerical codes, or to create new codes following new points of view, aiming to adequately simulate fluid flows and the related transport of physical properties. Additionally, the continuous improving of laboratory devices and equipment, which allow to record and measure fluid flows with a higher degree of details, induces to elaborate specific experiments, in order to shed light in unsolved aspects of the phenomena related to these flows. This volume presents conclusions about different aspects of calculated and observed flows, discussing the tools used in the analyses. It contains eighteen chapters, organized in four sections: 1) Smoothed Spheres, 2) Models and Codes in Fluid Dynamics, 3) Complex Hydraulic Engineering Applications, 4) Hydrodynamics and Heat/Mass Transfer. The chapters present results directed to the optimization of the methods and tools of Hydrodynamics.

How to reference
In order to correctly reference this scholarly work, feel free to copy and paste the following:

Dipankar Chatterjee (2011). Lattice Boltzmann Modeling for Melting/Solidification Processes, Hydrodynamics - Optimizing Methods and Tools, Prof. Harry Schulz (Ed.), ISBN: 978-953-307-712-3, InTech, Available from: http://www.intechopen.com/books/hydrodynamics-optimizing-methods-and-tools/lattice-boltzmann-modeling-for-melting-solidification-processes

INTECH
open science | open minds

InTech Europe
University Campus STeP Ri
Slavka Krautzeka 83/A
51000 Rijeka, Croatia
Phone: +385 (51) 770 447
Fax: +385 (51) 686 166
www.intechopen.com

InTech China
Unit 405, Office Block, Hotel Equatorial Shanghai
No.65, Yan An Road (West), Shanghai, 200040, China
中国上海市延安西路65号上海国际贵都大饭店办公楼405单元
Phone: +86-21-62489820
Fax: +86-21-62489821

IntechOpen